Journal of Materials and Environmental Science
ISSN : 2028-2508
e-ISSN : 2737-890X
CODEN : JMESCN

J. Mater. Environ. Sci., 2025, Volume 16, Issue 3, Page 451-471

http://www.jmaterenvironsci.com

Nanostructured CuO, ZnO, and CuO/ZnO Heterostructures via Acetate-Based Electrodeposition: Exploring Their Optoelectronic Properties for Potential Energy Harvesting Applications

Md. Suman Islam[1], Md. Sakib Ahmed[1], Jubayer Ahmmed Bappy[1], Md. Mahfujur Rahman[1], Mst. Ema Khatun[1], Parvaj Rana[1], Abdul Kuddus[2], Abu Bakar Md. Ismail[1*]

[1]Solar Energy Laboratory, Department of Electrical & Electronic Engineering, University of Rajshahi, Rajshahi 6205, Bangladesh

[2]Ritsumeikan Global Innovation Research Organization, Ritsumeikan University, Shiga, Japan.

**Corresponding author, Email address: ismail@ru.ac.bd*

Received *03 Feb 2025,*
Revised *25 Feb 2025,*
Accepted *02 Mar 2025*

Keywords:
- ✓ CuO/ZnO Heterostructures;
- ✓ Nanocrystals;
- ✓ Acetate-electrolyte;
- ✓ Electrodeposition;

Citation*: Islam S. M., Ahmed S. M., Bappy A. J., Rahman M., Rahman M., Khatun E. M., Rana P., Kuddus A., Ismail M.B.A. (2025) Nanostructured CuO, ZnO, and CuO/ZnO heterostructures via acetate-based electrodeposition: exploring their optoelectronic properties for potential energy harvesting applications, J. Mater. Environ. Sci., 16(3), 451-471*

Abstract: This work explores a sustainable and facile electrodeposition approach to fabricate nanostructured CuO, ZnO, and CuO/ZnO heterostructures for energy harvesting applications. Using ethylene glycol-based acetate salt electrolytes, CuO and ZnO thin films were separately deposited on fluorine-doped tin oxide (FTO) substrates. The CuO/ZnO heterostructure was deposited using two different route namely, sequential and in-situ. In sequential deposition ZnO is deposited first and then CuO is deposited on ZnO by changing electrolyte. Whereas, binary electrolyte of Cu-acetate and Zn-acetate was utilized for CuO (deposition potential of -0.63V) first and then ZnO (depositon potential of -1.32V) deposition in in-situ process. The XRD studies showed that separately deposited CuO polycrystalline nature with average crystalline size 25.81 nm but ZnO owning monocrystalline nature with 24.45 nm crystal size. In the heterostructure CuO and ZnO both possess polycrystalline nature with crystal size 31.18nm and 13.51 nm, respectively. The FTIR also confirmed the presence of Cu-O and Zn-O stretching vibration peaks for CuO, ZnO and CuO/ZnO structures. Dense and compact morphology for the CuO, ZnO and CuO/ZnO heterostructure deposited from sequential and in-situ deposition were revealed by the SEM study. The tunability of optoelectronic properties with deposition time was inspected by UV-VIS and thickness profiling of CuO and ZnO films. The in-situ electrodeposition of CuO/ZnO structure from the binary acetate electrolyte demonstrates a streamlined, cost-effective method for scalable synthesis, minimizing contamination and enhancing interfacial quality. This work highlights the effectiveness and tunability of acetate-assisted electrodeposition as an eco-friendly, scalable route for next-generation energy harvesting applications.

1. Introduction

Energy harvesting technologies are at the forefront of addressing global energy demands sustainably, with a particular focus on developing efficient and cost-effective materials for photovoltaic and optoelectronic applications (Vasiliev *et al.*, 2019). In recent years, the quest for sustainable and cost-effective alternatives in energy-related applications has driven researchers toward exploring earth-abundant metal oxides. Among these, transition metal oxides copper oxide (CuO) and zinc oxide (ZnO) have emerged as promising candidates due to their abundance, nontoxicity, and excellent semiconducting properties (Li *et al.*, 2010), (Suleiman *et al.*, 2013), (Bahnasawy *et al.*, 2022) , (Alshahateet *et al.*, 2024). Zinc oxide (ZnO) and copper oxide (CuO) are widely studied materials for

energy devices due to their complementary electronic and optical properties. ZnO, with its wide bandgap (~3.37 eV) and high electron mobility, is an excellent n-type semiconductor, offering strong optical transparency and efficient charge transport, making it suitable for photovoltaic and photocatalytic applications (Ozer *et al.*, 2024), (Slimani *et al.*, 2020). Conversely, CuO, a p-type semiconductor with a narrower bandgap (~1.2-1.9 eV), exhibits high absorption in the visible range and efficient hole transport properties, essential for light harvesting and charge separation in heterojunction structures (Ozer *et al.*, 2024), (Costas *et al.*, 2022). Their stability, abundance, and environmentally benign nature further enhance their potential for sustainable energy technologies (Bekru *et al.*, 2022). The integration of ZnO and CuO into heterostructures combines the high electron mobility of ZnO with the superior hole transport properties of CuO, making them ideal for applications such as solar cells, photodetectors, and photocatalysis (Kidowaki *et al.*, 2012), (Costas *et al.*, 2020). (Murzin *et al.*, 2022). Additionally, the band gap alignment in CuO/ZnO heterostructures facilitates efficient energy conversion by minimizing recombination losses (Kaphle *et al.*, 2020). Among various thin-film fabrication methods, such as sol-gel, hydrothermal synthesis, thermal oxidation, and chemical bath deposition, electrodeposition stands out due to its unique advantages (Asim *et al.*, 2014), (Kumar *et al.*, 2014). (Escorcia-Díaz *et al.*, 2023). Most of them, often involve energy-intensive processes, high temperature, complex vacuum, lack of thickness and composition controllability, or environmentally threatening issues (Pedersen *et al.*, 2021). While, electrodeposition has emerged as a scalable and sustainable technique, enabling precise control over film morphology and composition while minimizing material waste (Al-Katrib *et al.*, 2023), (Badalbayli *et al.*, 2024). In electrodeposition an electric current passing through an electrolyte solution containing metal ions, while the metal ions migrate towards the electrode surface where reduction occurs, resulting in the growth of a thin uniform films. This electrochemical method is particularly advantageous due to its simplicity, low-temperature processing and compatibility with diverse substrates, including flexible and transparent conductive materials (Oliveira *et al.*, 2016). Additionally, it allows fine-tuning of film properties, such as crystallinity, thickness, and morphology, by adjusting deposition parameters such as voltage and electrolyte composition (Pena *et al.*, 2018). These features make electrodeposition a cost-effective and environmentally friendly alternative to conventional techniques. Further, an ability to form efficient heterostructures with favorable band alignment, which enables effective charge separation and improved carrier mobility, has expanded their utility in energy conversion devices (Shaikh *et al.*, 2020). Specifically, one-pot electrodeposition offers an additional advantage by streamlining the fabrication of heterostructures devices. Instead of depositing individual layers sequentially, a common binary electrolyte can be employed to simultaneously deposit ZnO and CuO, reducing processing steps and potential contamination (Izaki *et al.*, 2014). This approach aligns with the principles of green chemistry by enhancing efficiency and sustainability in material synthesis (Sydnes *et al.*, 2014), (Casabán *et al.*, 2012). The electrodeposition of CuO/ZnO heterostructures offers distinct advantages for energy harvesting due to their complementary electronic and optical properties. ZnO, with its wide band gap (~3.37 eV) and high electron mobility (~200 $cm^2/V \cdot s$), enhances charge transport and offers strong optical transparency, making it ideal for photovoltaic and photocatalytic applications (Cui *et al.*, 2010), (Jeong *et al.*, 2007).

In contrast, CuO, a p-type semiconductor with a narrower bandgap (~1.21-1.9 eV), exhibits high light absorption (10^3-10^4 cm^{-1} in the visible range) and efficient hole transport, which are crucial for effective charge separation in heterostructures (Chatterjee *et al.*, 2016), (Jrajri *et al.*, 2021). The synergy of these materials enhances light harvesting and energy conversion, making ZnO/CuO heterostructures highly promising for sustainable energy technologies (Bekru *et al.*, 2022). The use of

acetate salt electrolytes in electrodeposition is particularly advantageous due to their ability to stabilize precursor ions and facilitate uniform nucleation (Amiri *et al.*, 2021). Acetate-based systems not only ensure reproducibility but also allow fine-tuning of deposition parameters, such as pH and potential, to achieve desired film properties (Stalcup *et al.*, 2024). Cyclic voltammetry (CV) plays a crucial role in optimizing deposition potentials, as it provides insights into the redox behavior of Zn and Cu species in the electrolyte (Shin *et al.*, 2015). The choice of fluorine-doped tin oxide (FTO) as a substrate in this study is motivated by its excellent optical transparency and electrical conductivity, which are critical for efficient charge transport in energy harvesting devices (Muthukumar *et al.*, 2013). The combination of FTO substrates with electrodeposited ZnO/CuO heterostructures ensures robust interfaces, which are essential for device stability and performance (Ghimire *et al.*, 2023). The simultaneous use of acetate-derived precursors in ethylene glycol and sodium acetate buffering is rarely explored in the literature for the electrodeposition of CuO/ZnO heterostructure, which may open a pathway for fine-tuning the optoelectronic performance of CuO/ZnO heterostructures. In this study, we present a novel one-pot electrodeposition method for fabricating ZnO and CuO heterostructure on FTO-coated glass substrates. Two methodologies were explored: (i) separate deposition of ZnO and CuO from distinct solutions and (ii) simultaneous (in-situ) deposition from a mixed electrolyte containing zinc acetate, copper acetate, and sodium acetate trihydrate. The influence of deposition parameters, such as potential, temperature, and pH, on film morphology and optoelectronic performance was systematically investigated. The findings of this study highlight the potential of acetate salt electrolyte-assisted electrodeposition as a sustainable and scalable approach for synthesizing high-quality CuO/ZnO heterostructures, offering an environmentally friendly alternative to conventional fabrication methods. By addressing key challenges in material synthesis and integration, this work contributes to the development of next-generation optoelectronic devices retaining global sustainability goals.

2. Materials and methods

2.1 Materials

Zinc acetate dihydrate ($Zn(C_2H_3O_2)_2.2H_2O$) (purity>99%), Copper (II) acetate $(CH_3COO)_2Cu.H_2O$ (purity>99%), Sodium acetate trihydrate $CH_3COONa.3H_2O$ (purity>99%), Ethylene glycol, and acetone (C_3H_6O) were used for the ZnO, CuO, CuO/ZnO synthesis using Electrodeposition technique, were commercially purchased from Sigma-Aldrich Company and used without further purification. Sodium Acetate Trihydrate ($CH_3COONa·3H_2O$) utilized as buffering Agent and ion Source. Sodium acetate stabilize the pH of the electrolyte solution during the electrodeposition process. The acetate ion (CH_3COO^-) acts as a buffering species, resisting pH changes caused by the electrochemical reactions occurring at the electrode surface retaining an optimized pH range (~5.68) to achieve controlled growth and prevent the formation of undesirable phases like hydroxides. Sodium Acetate also contributes ZnO, CuO precursors acetate's ions, which can interact with the metal cations (Zn^{2+} and Cu^{2+}), facilitating uniform and stable deposition of ZnO and CuO layers (Mezine *et al.*, 2018). On the other hand, Ethylene Glycol ($C_2H_6O_2$) (EG) acts as complexing/chelating agent, forming stable complexes with Zn^{2+} and Cu^{2+} ions. This slows down the release of metal ions at the electrode surface, promoting uniform deposition and reducing the risk of agglomeration or dendrite formation. It also supports to control viscosity. It increases the viscosity of the electrolyte, which improves ion transport stability and reduces convection currents during electrodeposition with uniform growth of metal oxides, MOs (M= Zn, Cu) films. Additionally, EG support to modulate the reduction potentials of the metal ions, improving the selectivity of ZnO and CuO deposition within the desired voltage range.

2.2 Electrodeposition of ZnO, CuO thin films and their heterostructures films

The nanostructure ZnO and CuO thin films were fabricated employing by electrochemical deposition method (known as galvanostatic plating system) on precleaned fluorine-doped tin oxide (FTO) coated glass (F-Sn_2O, 2.2 mm and 7Ω/sq^{-1}) with sizes of 4×1.5 cm^2. Substrate cleaning was executed by sequential dipping in DI water, acetone, DI water under sonication, each step for 10 minutes, followed by pre-heating at 100 °C for 10 minutes in vacuum chamber (~10^{-3} pA). Pre-heating improves adhesion and stabilize surface properties. Three-electrode cell system (Admiral Instruments Squidstat Plus Potentiostat operate by Squidstat User Interface (SUI)) has been adopted; FTO was utilized as working electrodes (WE), a Pt grid as counter electrode (CE) and a silver/silver chloride (Ag/AgCl) as reference (RE). All substrates were sequentially cleaned in an ultrasonic cleaner with DI water, acetone and DI water, each for 10 minutes and dry by blower. The schematic, camera image of the electrodeposition and homemade pre-heating set-up is demonstrated in **Figure 1.**

The cell was contacted with an 0.3 M acetate solution (zinc acetate, or copper acetate) and 0.2 M Sodium acetate trihydrate, dissolved in 40 ml ethylene glycol at fixed pH (4.68 for ZnO, 5.68 for Cu_xO). The bath temperature was maintained at 70˚C. Deposition potential of -1.325 V for ZnO and -0.63 V for CuO were applied and controlled by in-situ Cyclic Voltammetry (C-V) observation. Electrodeposition was executed for varying period of 2min, 5min, 10 min for both of ZnO and CuO films. For CuO/ZnO heterostructure films, two methodologies were employed: (i) separate electrodeposition of ZnO and CuO from distinct electrolyte solutions of 0.3M zinc acetate, 0.3M copper acetate, and 0.2M sodium acetate trihydrate, while (ii) simultaneous deposition performed from a buffer solution containing both Zn and Cu-acetate salts. The overall process was executed under computer program controlled in-situ cyclic voltammetry observations.

2.3 Characterization

The morphology and composition of the deposited films were analyzed using scanning electron microscopy (SEM) and energy-dispersive X-ray spectroscopy (EDS). X-ray diffraction (XRD) was employed to study the crystal structure of the ZnO and CuO layers and CuO/ZnO heterostructure films. UV-Visible spectrophotometry was used to evaluate the optical properties of the films while the optical bandgap determined from the respective absorbance in a wavelength range of 360-1100 nm., and their electrochemical characteristics were assessed using cyclic voltammetry and current-voltage (I-V) measurements performed under simulated AM1.5G solar illumination.

In Electrodeposition, the flow of current during electrodeposition is proportional to the deposition rate, and this relationship is typically governed by *Faraday's Law of Electrolysis* (Walsh *et al.*, 1991). The equation linking the current (II) to the deposition rate (mm) is:

$$r = \frac{I.\ t.\ M}{z.\ F} \qquad \textbf{Eqn. 1}$$

Where, *m*, is mass of the deposited material (grams, g), *I* is the current (amperes, A), *t* is Time (seconds, s). *M* is molar mass of the deposited substance (grams/mole), z is number of electrons involved in the electrochemical reaction, *F* is Faraday's constant (96485 C/mol), charge per mole of electrons). The deposition rate (*r*) in terms of mass per unit time can be expressed as:

$$r = \frac{I.\ M}{z.\ F} \qquad \textbf{Eqn. 2}$$

This indicates that the deposition rate is directly proportional to the current ($r \propto I$), assuming constant molar mass (*M*) and reaction stoichiometry (*z*).

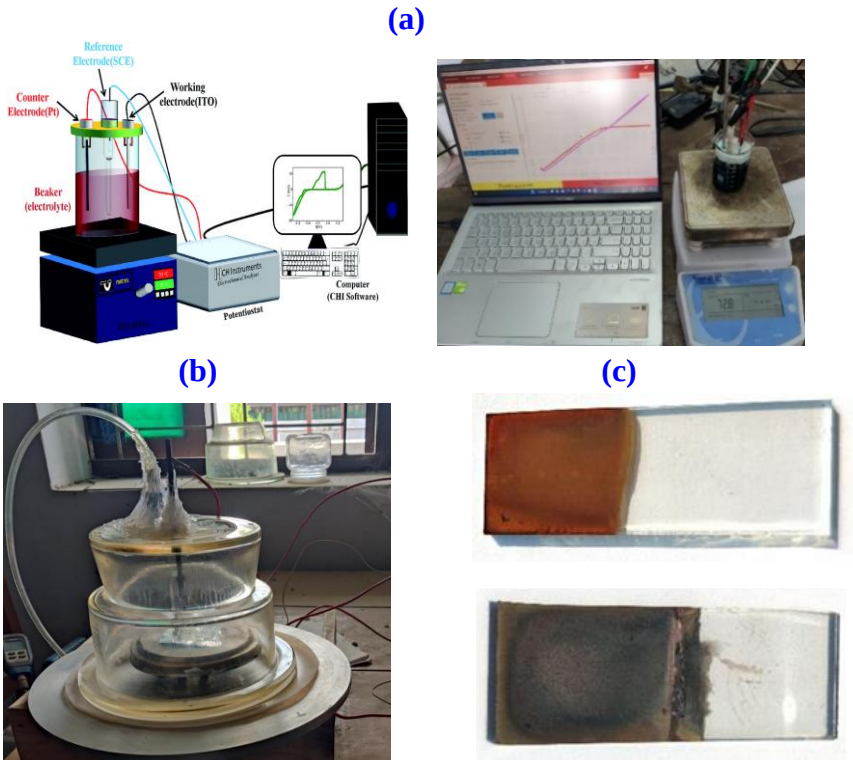

Figure 1: (a) Schematic of the electrodeposition, **(b)** homemade pre-heating vacuum chamber and **(c)** electrodeposited CuO films (before and after annealing at 400 °C for 45 minutes).

3. Results and Discussion

3.1 Growth and properties of ZnO, and CuO thin films

3.1.1 Thickness study of CuO, and ZnO thin films

Figure 2a, and **b** illustrate the deposition rates of CuO and ZnO thin films fabricated via electrodeposition on FTO substrates using 0.3 M copper (II) acetate and zinc acetate, respectively. In both cases, the thickness of the films increases progressively with deposition time, showcasing distinct linear and non-linear trends indicative of their deposition mechanisms. For CuO, the deposition profile reveals an accelerating growth rate over time, attributed to the nucleation and growth kinetics characteristic of copper oxide phases (**Figure 2a**). The use of copper (II) acetate as a precursor, alongside sodium acetate as a pH buffer, facilitates the controlled reduction of Cu^{2+} ions at the cathode, forming CuO layers. This behavior aligns with literature observations where copper acetate precursors are used in electrodeposition, though their use in combination with sodium acetate is relatively less explored, enhancing the novelty of this work (Jrajri *et al.*, 2021). CuO, with its inherent cation deficiency, conventionally exhibits p-type conductivity due to hole generation in the lattice, making it an attractive candidate for hole transport layers in optoelectronic devices. On the other hand, a linear deposition trend, indicating steady-state kinetics typical for ZnO electrodeposition for ZnO (**Figure 2b**). The uniformity of growth is achieved by the reduction of Zn^{2+} ions to Zn atoms, followed by oxidation to ZnO on the FTO substrate. The application of zinc acetate as a precursor is well-documented, yet the optimization of its molarity and deposition parameters, as shown here, underscores the reproducibility and high deposition rates compared to prior studies (Šulčiūtė *et al.*, 2012). ZnO's *n*-type conductivity, stemming from oxygen vacancies and interstitial zinc, complements the p-type CuO, making the two materials suitable for heterojunction applications. The contrasting deposition profiles of CuO and ZnO highlight their differing ion reduction mechanisms and nucleation kinetics.

While CuO shows an exponential growth characteristic of a nucleation-limited process, ZnO's linear trend is governed by diffusion-controlled deposition.

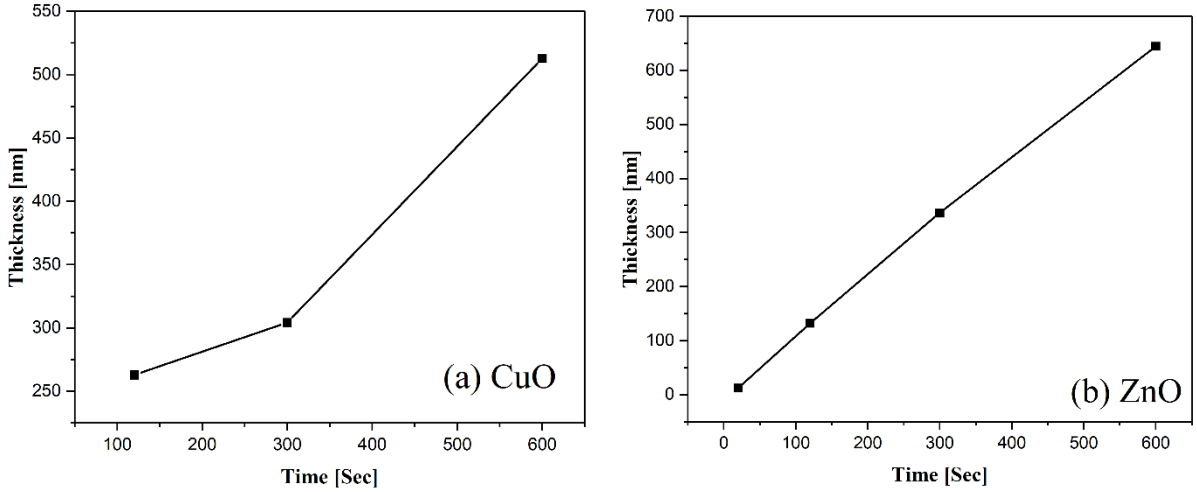

Figure 2. Deposition rate of CuO and ZnO thin films deposited on FTO-coated glass substrate.

This distinction is critical for achieving tailored film thickness and morphology for device applications. Thus, this work demonstrates simultaneous use of acetate-derived precursors and sodium acetate buffering, offering precise control over deposition rates and film properties. Such a combination is underexplored in the literature and opens pathways for fine-tuning the optoelectronic performance of CuO/ZnO heterostructures, revealing potential advancements in photovoltaic, sensing, and photocatalytic applications due to the optimized film quality and thickness uniformity.

3.1.2 Optical properties of CuO, and ZnO thin films

Figure 3 depict the deposition rate of electrodeposition of CuO/FTO and ZnO/FTO thin films using 0.3 M Cu-Acetate and Zn-acetate, respectively, measured over the wavelength range of 300–900 nm. The transmittance spectra for CuO films deposited for 2 minutes and 5 minutes exhibit an inverse correlation with deposition time (**Figure 3a**). The thinner film (2 min) demonstrates higher transmittance, peaking at approximately 26% at 900 nm, whereas the thicker film (5 min) shows reduced transmittance (~12% at 900 nm). This is attributed to the increased optical density and scattering effects in the thicker film. The absorbance spectra illustrate that films deposited for 5 minutes exhibit stronger absorption in the visible region (~400–800 nm), peaking at around 700 nm. The thinner film shows a weaker absorption peak at a similar wavelength, indicating the influence of film thickness on light-matter interaction. The pronounced absorption in the visible region is consistent with the semiconductor nature of CuO, known for its narrow bandgap (~1.2–2.1 eV depending on stoichiometry). This behavior aligns with prior reports on CuO-based films used for photocatalysis and photovoltaics, where increased thickness enhances light absorption but at the expense of transparency (Hssi *et al.*, 2020), (Aswada *et al.*, 2021). Compared to ZnO films analyzed earlier, CuO exhibits much stronger absorption in the visible range, consistent with its lower bandgap. The transmittance of CuO is also substantially lower, underscoring its potential for light-harvesting applications. For applications requiring optimized transparency and absorption balance, precise control of deposition time and film thickness is crucial. These optical properties render CuO thin films promising candidates for visible-light-driven photocatalysis, solar cells, and optoelectronic devices. The tunability of thickness through deposition time offers a pathway to tailor their performance for specific applications. For example,

thinner films are advantageous for optoelectronic devices requiring transparency, whereas thicker films benefit photocatalytic efficiency by enhancing light absorption. The transmittance increases steadily from ~300 nm toward longer wavelengths in the visible region, reaching over 90% for the film deposited for 30 seconds and ~80% for the 1-minute deposition (**Figure 3b**).

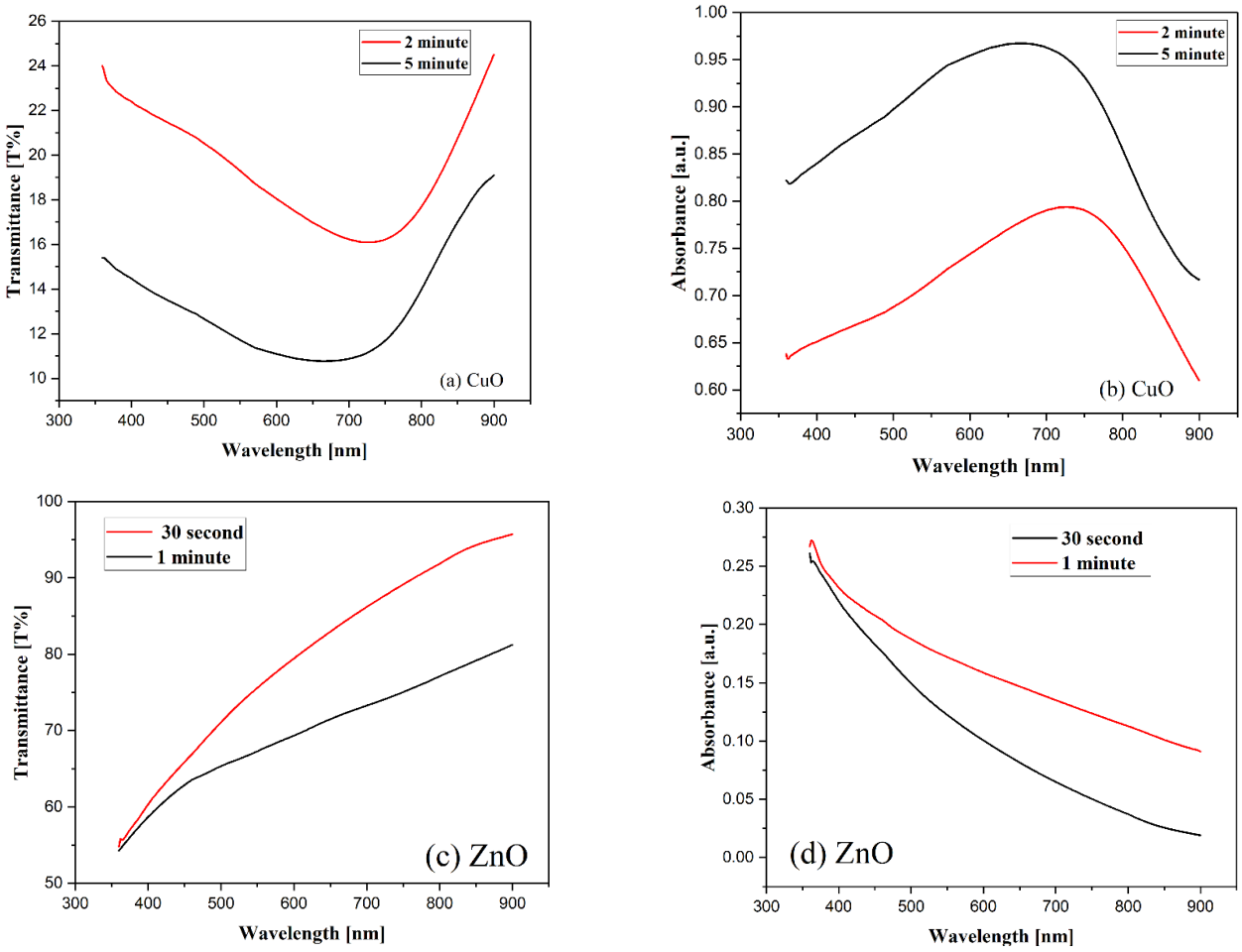

Figure 3. Transmittance and Absorbance spectra of **(a)** & **(b)** CuO and **(c)** & **(d)** ZnO thin films.

The film deposited for a longer time (1 minute) shows lower transmittance across the spectrum, attributed to the increased film thickness, which enhances light scattering and absorption. On the other hand, both spectra show an absorption edge at around 375–400 nm, characteristic of ZnO's wide bandgap (~3.2–3.4 eV). The film deposited for 1-minute exhibits higher absorbance, consistent with greater material deposition, indicating an increased density of light-absorbing ZnO nanostructures. A sharp absorption edge indicative of good crystallinity, as suggested in studies correlating bandgap properties with structural quality compare to previously reported ZnO thin films grown via electrodeposition or other solution-based methods (Siregar *et al.*, 2023). The reduction in transmittance for the longer deposition time increases film thickness, impacts optical properties by introducing light scattering due to surface roughness and larger particle sizes, which is align with earlier reports (Tolosa *et al.*, 2019). The distinct optical behavior of these ZnO films makes them suitable for applications requiring high transparency and efficient light absorption, such as UV filters, photocatalytic systems, and transparent electrodes. The tunability of their optical properties through deposition time highlights the versatility of the synthesis approach.

Figure 4 FTIR spectrum (Figure) shows distinct absorption peaks, which provide insights into the chemical bonding, structural integrity, and functional groups present in the CuO thin films deposited on an FTO substrate.

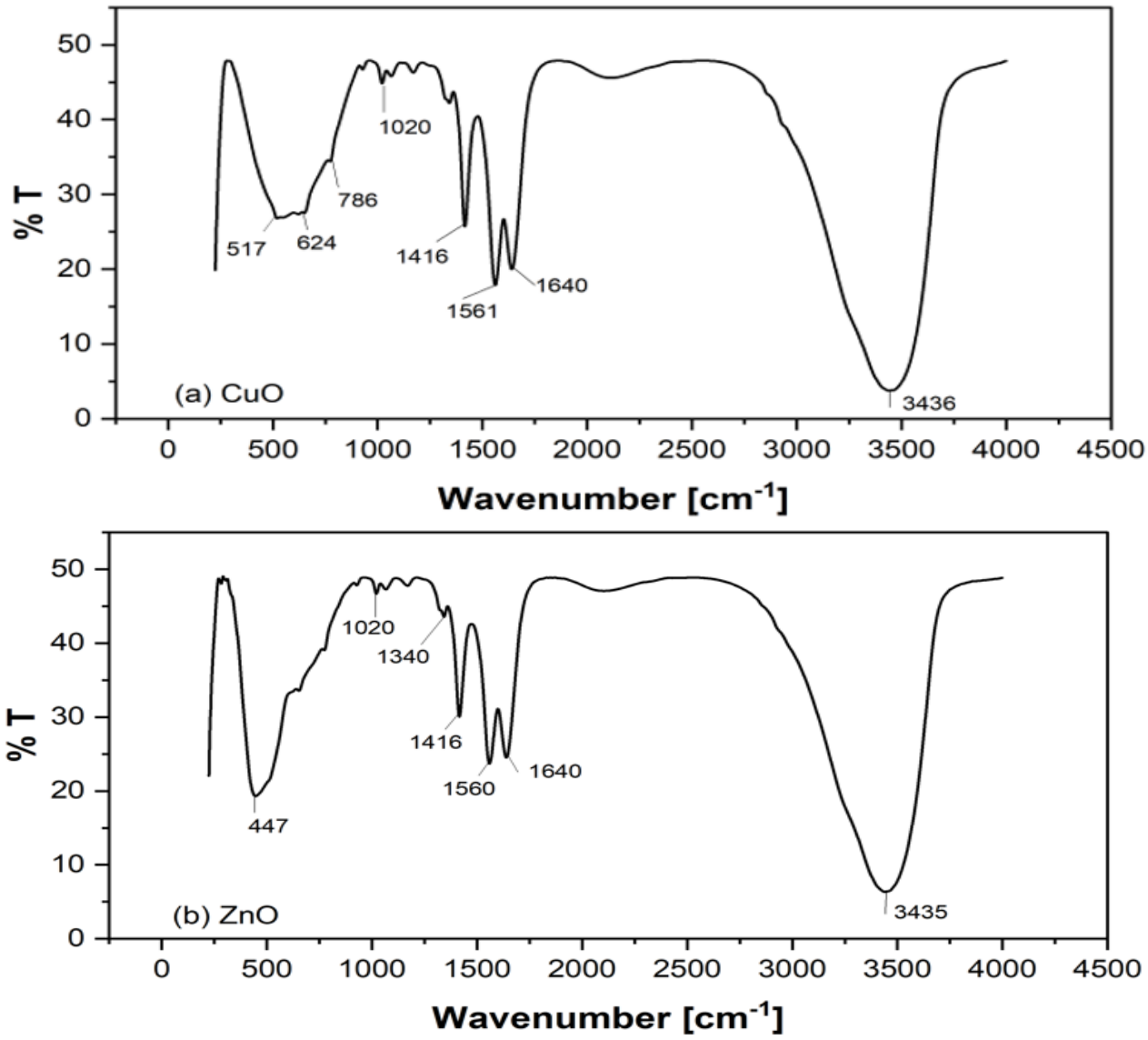

Figure 4. FTIR of **(a)** CuO and **(b)** ZnO thin films deposited on transparent FTO substrate.

In **Figure 4a,** the vibration-related peak at 3436 cm^{-1} corresponds to the stretching vibrations of hydroxyl (O–H) groups, indicating the presence of adsorbed water or surface hydroxyl groups on the thin film. Such features are commonly observed in CuO thin films due to surface interactions during deposition and exposure to ambient moisture (Dehaj *et al.*, 2019), (Imani *et al.*, 2020). The C=C stretching at 1640 cm^{-1} is attributed to C=C bonds, may be from organic residual components. The C=O and C–H Vibrations at 1561 cm^{-1} and 1416 cm^{-1} correspond to the stretching of carbonyl groups C=O and bending of aliphatic C–H bonds. Their presence may arise from residual acetate groups used in the deposition process. Similar features have been noted in studies involving acetate precursors (Deora *et al.*, 2019). The C–O Stretching at 1020 cm^{-1} corresponds to C–O stretching vibrations, likely from incomplete decomposition of acetate precursors. Similar results have been observed in electrodeposited films (Dehaj *et al.*, 2019). The Cu–O vibrations at 786, 624, and 517 cm^{-1} are assigned

to Cu–O stretching vibrations, confirming the formation of CuO phases in the heterostructure. Specifically, the band at 624 cm^{-1} is characteristic of CuO (Bouachma *et al.*, 2021), (Varughese *et al.*, 2020). The observed Cu–O peaks match well with those reported studies of electrodeposited CuO thin films, demonstrating the successful formation of a CuO phase structure. Additionally, the presence of residual acetate groups (C–O, C=O, and C–H vibrations) is consistent with previous works. Thus, the combination of specific Cu–O peaks (786, 624, 517 cm^{-1}) in this work while the general features align with prior studies, is indicative of a robust deposition method capable of forming a CuO phase structure with controlled morphology. This CuO phase is critical for tuning optical and electronic properties in photocatalysis, offering potential advantages CuO films.

Figure 4b The FTIR spectrum of the ZnO thin films, as depicted in, reveals distinct vibrational bands that correspond to the chemical bonding and structural characteristics of the material. The absorption peak around 3436 cm^{-1} is indicative of O-H stretching vibrations, often attributed to the presence of adsorbed water molecules or hydroxyl groups on the film surface. This suggests some degree of surface hydration, a feature common in ZnO thin films due to their polar nature. Similar studies have reported such peaks for ZnO thin films deposited using sol-gel or hydrothermal methods. The peak at approximately 1640 cm^{-1} corresponds to H-O-H bending vibrations, further confirming the presence of moisture or water molecules in the film structure. This aligns with findings in related works, where residual moisture in ZnO layers is common during low-temperature fabrication processes (Mia *et al.*, 2017). The peak at 1559 cm^{-1} is likely due to C=O stretching vibrations, possibly from residual organic precursors used during the synthesis. Such bands have been observed in ZnO thin films fabricated via acetate-based precursor solutions. The strong absorption band at 447 cm^{-1} represents the Zn-O stretching mode, confirming the successful formation of ZnO. This peak is characteristic of Zn-O bonds and has been widely reported in the literature for ZnO thin films (Khan *et al.*, 2016). Peaks at 1020.99 cm^{-1} and 1416.05 cm^{-1} associated with C-O stretching vibrations, indicating possible residuals from acetate precursors or incomplete combustion of organic ligands. Additional Peaks at lower frequencies, such as 303.01 cm^{-1}, may correspond to lattice vibrations or defect-related modes, however further analysis is required to confirm assignment. When compared with existing studies, the FTIR results confirm the characteristic Zn-O bonding (447 cm^{-1}), which is essential for validating the material's purity and crystallinity. The presence of additional peaks such as C=O and O-H bands highlights the influence of synthesis conditions, particularly the precursor type and deposition parameters (Khan *et al.*, 2011). These findings underscore the importance of optimizing precursor ratios and deposition conditions to minimize unwanted residuals, thereby enhancing the material's photocatalytic or optoelectronic performance.

3.1.3 Structural properties of CuO, and ZnO thin films

Figure 5 depicts the XRD spectra of CuO and ZnO thin films deposited on FTO substrates via electrodeposition. The FTO/CuO sample shows prominent peaks at 35.5° and 38.7°, attributed to the (-111) and (111) planes of monoclinic CuO (JCPDS #48-1548) (**Figure 5a**) (Siddiqui *et al.*, 2018). These peaks confirm the successful deposition of CuO in a polycrystalline structure. We calculated the average crystalline size by Debye-Scherrer's formula that is 25.81 nm which confirmed the nanocrystal structure is present on the electrodeposited CuO films (Parvaj Rana *et al.*, 2024). And the high intensity of these peaks suggests enhanced grain growth during deposition, which can improve light absorption and catalytic efficiency. In contrast, the spectrum for FTO/ZnO displays a distinct peak at 31.7°, corresponding to the (100) plane confirmed the monocrystallity of wurtzite ZnO (JCPDS #36-1451) (**Figure 5b**) (Jayswal *et al.*, 2018). This sharp peak reflects high crystallinity with crystal size 24.45

nm, which is vital for improving charge mobility in optoelectronic devices. The absence of secondary phases in the ZnO XRD pattern indicates phase purity, which is crucial for achieving optimal optical and electronic properties. The peak intensities and positions for both films align well with previously reported studies of ZnO and CuO thin films fabricated via different methods, including chemical vapor deposition and sputtering (Hajji *et al.*, 2024). However, the simplicity of the electrodeposition method used here offers a significant advantage, as it enables scalable and low-cost synthesis without compromising film quality. The current study's unique combination of ZnO and CuO with a one-pot deposition method simplifies the fabrication process, providing a more efficient route to achieving high-quality films suitable for photocatalysis and photovoltaics. The high crystallinity and phase purity of ZnO and CuO films confirmed by the XRD spectra enhance their potential for optoelectronic applications. The combination of *n*-type ZnO and *p*-type CuO in heterojunction devices can improve charge separation and photocatalytic activity, paving the way for their use in energy conversion systems, such as dye-sensitized solar cells (DSSCs) and water-splitting applications. This study contributes to the growing field of, cost-effective scalable nanostructured thin film deposition, offering a pathway toward sustainable growth.

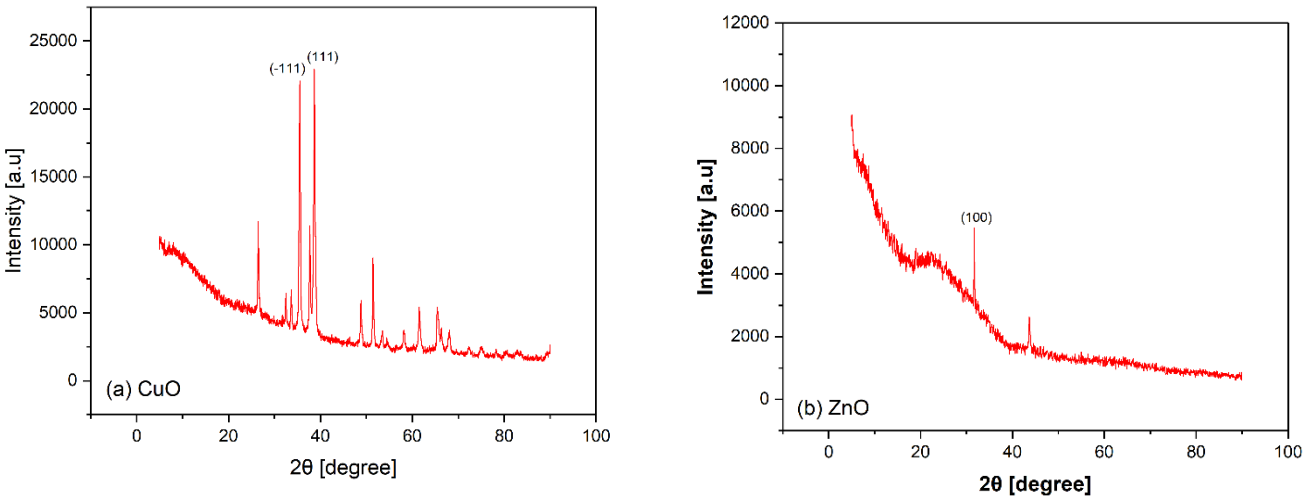

Figure 5. XRD of CuO and ZnO thin films deposited on transparent FTO substrate

3.2 Sequential electrodeposition of CuO/ZnO heterostructures films from distinct precursors solution

3.2.1 Surface morphology of FTO/CuO/ZnO heterostructures thin films from distinct precursors solution

Figures 6 shows SEM images of CuO/ZnO films. Initially, CuO film was deposited on FTO substrate on FTO at -0.63 V, subsequently ZnO on CuO coated FTO at -1.325 V, each of layers for 5 minutes forming FTO/CuO/ZnO vertically stacked heterostructure. Scanning electron microscopy (SEM) was employed to investigate the surface morphologies of the fabricated CuO/ZnO heterostructures films. This SEM image illustrates the cross-sectional morphology of the FTO/CuO/ZnO heterostructure film. The structure comprises a dense and uniform CuO layer deposited directly onto the FTO substrate, forming a robust p-type semiconductor base. Above the CuO layer, a ZnO layer with a granular, dome type flower-like microstructure morphology, which appears well-aligned and compact is visible, characteristic of an *n*-type semiconductor. The distinct interface between the CuO and ZnO layers, combined with the compact growth of both materials, indicates high-

quality fabrication suitable for photovoltaic and optoelectronic applications. The absence of voids or defects ensures good electrical and structural stability, essential for efficient charge transport. These findings align with recent studies on similar heterostructures (Saji *et al.*, 2013), (Lahmar *et al.*, 2017). FESEM images revealed (semi)spherical morphologies, in which particles were agglomerated and formed giant balls with diameters of about 1 μm. The particle size measurement displayed the FWHM of ~58.73 nm, which showed the mean diameter of 64.52 ± 21.48 nm. It appears that the particles were 2.25 times larger than the crystallites. The presence of the hydroxyls and carboxylates may lead to the aggregate formation due to the weak van der Waals forces and hydrogen bonds between the particles. Further elemental identification and analysis is found supportive to these observations.

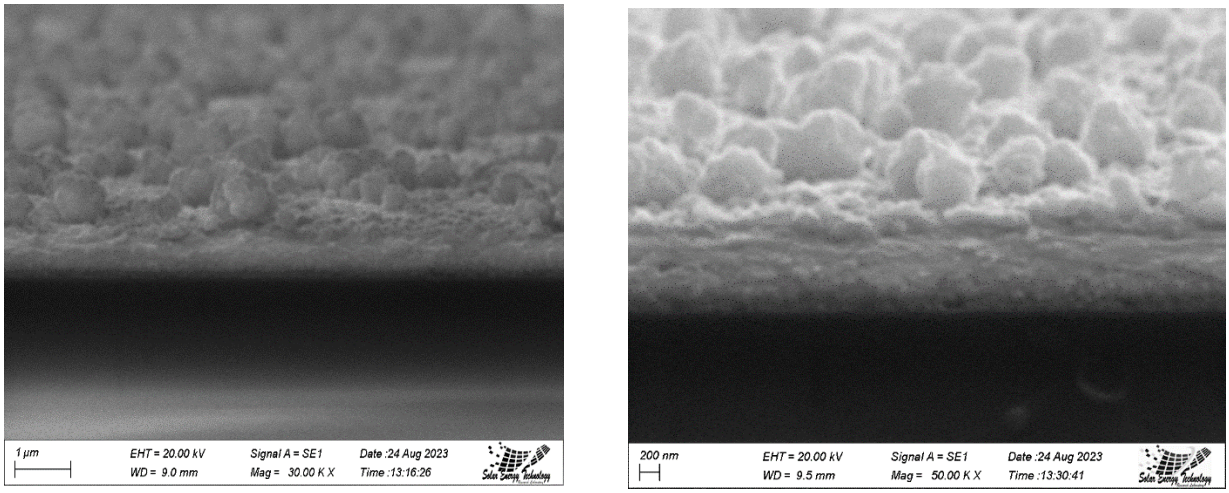

(a) **(b)**

Figure 6. SEM images **(a)** Mag. of 30X and **(b)** 50X of sequentially electrodeposited FTO/CuO/ZnO heterostructure.

3.2.2 Compositional properties of FTO/CuO/ZnO heterostructures thin films from distinct precursors solution

Figure 7 depicts characteristic vibrational modes of sequentially electrodeposited ZnO/CuO films on FTO substrates. The peak of 3415 cm^{-1} corresponds to the stretching vibration of hydroxyl (O–H Stretching) groups, indicative of absorbed water or hydroxyl ions. Its presence is crucial as surface hydroxyls often play a role in photocatalysis by facilitating charge separation and trapping reactive species. Comparable findings from previous works highlight the role of surface hydroxyls in enhancing the photocatalytic efficiency of nanostructured oxides. This minor peak of 2071 cm^{-1} (C≡C or C≡N Stretching) suggests possible contamination during the deposition process or residual precursor compounds. Its reduction or absence in similar studies correlates with better material purity and improved optoelectronic performance. The sharp peak at 1618 cm^{-1} (C=O Stretching) corresponds to carbonyl groups, potentially originating from acetate precursors. Residual acetate impacts the electronic properties by introducing mid-gap states, which may influence charge transport while the peak of 1384 cm^{-1} associated with vibrational modes of residual organic species (C–H Bending). The peak at 1122 cm^{-1} (Zn–O Stretching confirms the presence of ZnO. The Zn–O vibrational modes are central to the optoelectronic properties of ZnO, including its role in UV absorption and electron transport. The peaks at 753 cm^{-1} and 655 cm^{-1} (Cu–O vibrations) correspond to Cu–O stretching vibrations, confirming the CuO phase. Copper oxide's *p*-type conductivity enhances its suitability for heterojunctions with ZnO, forming efficient charge transport layers. Notably, the peak at 604 cm^{-1}

(ZnO lattice mode) is consistent with ZnO's wurtzite structure. Its presence, along with the Cu–O vibrations, corroborates the successful formation of a CuO/ZnO heterostructures. The identified peaks confirm the coexistence of ZnO and CuO phases, essential for heterostructures. These structures enable effective separation of photogenerated carriers, improving photocatalytic and photovoltaic performance. This spectrum aligns with those reports, by Zhang et al. (2020) and Gupta et al. (2019) demonstrate how tailored electrodeposition parameters and annealing improve the optical and structural properties of CuO/ZnO films, showcasing a scalable deposition route (Zhang *et al.*, 2023), (Hussain *et al.*, 2011). This characterization confirms the structural and chemical features critical for photocatalytic, sensing, or optoelectronic applications.

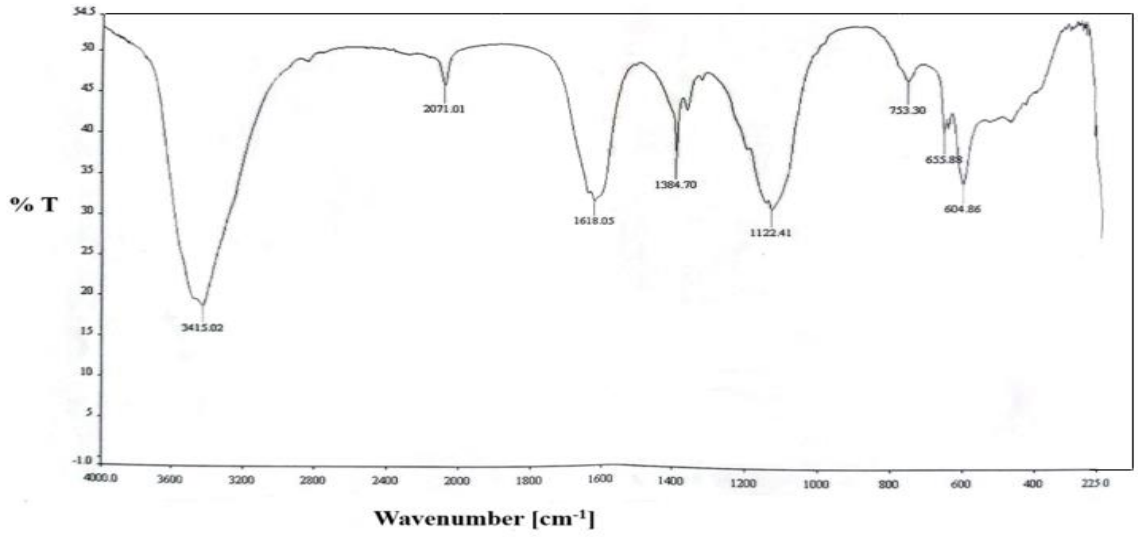

Figure 7. FTIR spectrum of sequentially electrodeposited FTO/CuO/ZnO heterostructures films from distinct Zn-and Cu-acetate precursors solutions.

3.3 CuO/ZnO heterostructures films from common Zn- and Cu-acetate's buffer solution

3.3.1 Surface morphology of FTO/CuO/ZnO heterostructures thin films from Zn-and Cu-acetate's buffer solution

Figure 8 shows SEM images of electrodeposited FTO/CuO/ZnO heterostructures thin films fabricated using Zn-acetate and Cu-acetate precursor buffer solutions. These heterostructures were prepared via simultaneous deposition from a buffer solution containing 0.3M zinc acetate, 0.3M copper acetate, and 0.2M sodium acetate trihydrate on FTO at a controlled potential. The cross-sectional SEM images reveal a well-defined bilayer structure, where CuO and ZnO are co-deposited to form a *p-n* heterostructures. The CuO component, identifiable by its compact and dense morphology, acts as the *p*-type semiconductor, providing a stable and robust foundation. Concurrently, the ZnO phase grows with a granular, partial pyramid-like microstructure characteristic of *n*-type semiconductors, facilitating enhanced surface area and light-scattering properties. The intimate and continuous interface between CuO and ZnO layers suggests excellent interfacial adhesion, which is beneficial for ensuring efficient charge separation and transport. This structural integrity is critical for improving device performance, particularly in energy harvesting applications. When compared to sequentially deposited heterojunctions, the simultaneous deposition method offers significant advantages, including enhanced material homogeneity, reduced fabrication time, and better interlayer connectivity. The buffer solution containing sodium acetate trihydrate acts as a stabilizing agent, optimizing the deposition conditions for the concurrent growth of CuO and ZnO phases. Such a controlled environment promotes the

formation of high-quality, defect-free interfaces crucial for high-efficiency energy devices, including photovoltaic cells, photoelectrochemical devices, and thermoelectric systems. The simultaneous electrodeposition approach not only simplifies fabrication but also enhances the structural and functional properties of the films. The granular ZnO morphology, coupled with the dense CuO, ensures efficient light absorption, charge carrier separation, and transport, making this heterostructure highly suitable for next-generation optoelectronic and energy devices. Furthermore, the cost-effectiveness and scalability of the simultaneous deposition process underscore its practicality for large-scale fabrications.

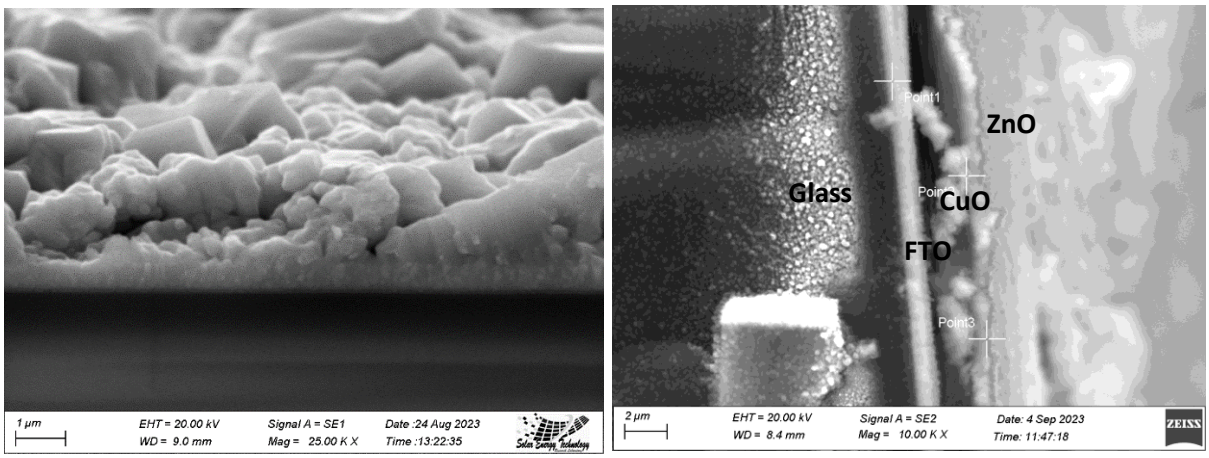

(a) **(b)**

Figure 8. SEM images of **(a)** surface and **(b)** cross-section of electrodeposited FTO/CuO/ZnO heterostructures from binary electrolyte composed of Zn-acetate and Cu-acetate and ethylene glycol.

3.3.2 Compositional properties of FTO/CuO-ZnO heterostructure thin films from buffer precursors solution

Figure 9 illustrates the FTIR spectrum of electrodeposited FTO/CuO/ZnO heterostructures films fabricated from a common Zn-acetate and Cu-acetate in ethylene glycol solution. The spectrum provides critical insights into the chemical composition and bonding characteristics of the synthesized films, confirming the successful co-deposition of CuO and ZnO. Broad peak at ~3421 cm^{-1} corresponds to the O–H stretching vibrations, indicating the presence of hydroxyl groups, likely due to adsorbed water molecules or hydroxide intermediates formed during the deposition process. The presence of these groups is commonly observed in metal oxide films synthesized via aqueous routes and plays a crucial role in the nucleation and growth of oxide layers (Jeong *et al.*, 2007). Peak at ~1600 cm^{-1} is attributed to H–O–H bending vibrations, further confirming adsorbed water on the film surface. The combination of hydroxyl and water-related peaks indicates a hydrated surface, which can impact the electrical and optical properties of the heterojunction. The peak at ~1384 cm^{-1} and ~1122 cm^{-1} corresponds feature arises from the symmetric stretching vibrations of COO^- and C–O group, suggesting residual acetate species from the precursor solution, due to residual organic components from the precursor's incomplete decomposition or intermediates, which is typical in films prepared via low-temperature aqueous methods (Filopoulou *et al.*, 2021). This refer the post thermal annealing is required to accelerate full decomposition, and reduce organic impurities, thus improve film crystallinity and stability.

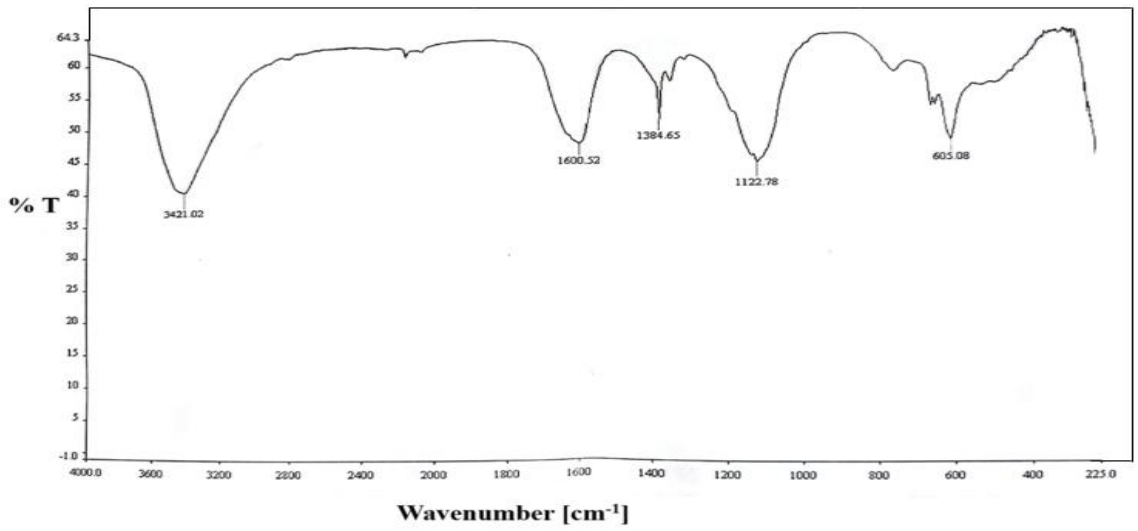

Figure 9. FTIR spectrum of electrodeposited FTO/CuO/ZnO heterostructure films from a common Zn-acetate and Cu-acetate precursors containing buffer solution.

Notably, a broad peak at ~660-600 cm^{-1} reflects the characteristic of metal–oxygen (M–O) stretching vibrations. Specifically, the peaks around ~660 cm^{-1} can be assigned to Cu–O bonds in CuO, while those near 600 cm^{-1} are attributed to Zn–O stretching in ZnO. These peaks confirm the successful incorporation and co-deposition of CuO and ZnO phases, forming a composite heterojunction structure (Siva *et al.*, 2020). The observed peaks further validate the structural and chemical integrity of the films, underscoring their potential for optoelectronic and energy applications. The single port simultaneous electrodeposition demonstrates an improved interlayer bonding and excellent interfacial compatibility, crucial for efficient charge transport at a reduced complexity, time, and cost, making the process strong potential for growth and subsequent applications. This study aligns with prior research that highlights the role of simultaneous deposition in producing defect-minimized interfaces and enhancing heterojunction performance for energy harvesting devices (Tran *et al.*, 2018).

Figure 10 shows the EDS spectrum elemental analysis of electrodeposited FTO/CuO/ZnO heterostructures films synthesized from a Zn-acetate and Cu-acetate precursor solution. **Table 1** summarizes corresponding weight and atomic percentages.

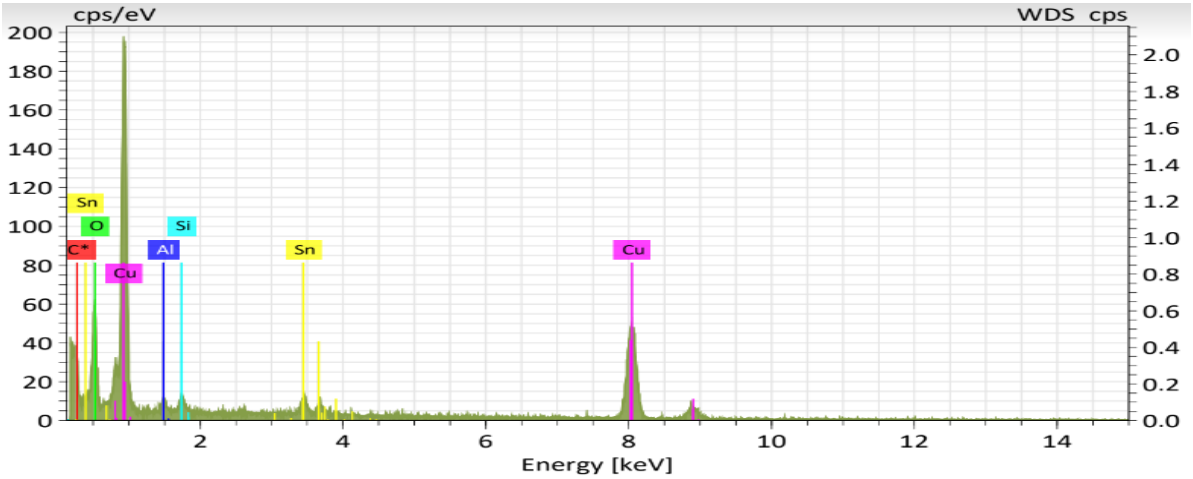

Figure 10. EDS spectrum of electrodeposited FTO/CuO/ZnO heterostructure films from a common Zn-acetate and Cu-acetate precursors solution.

Table 1. Summary of atomic percentages of electrodeposited FTO/CuO/ZnO heterostructures films from a common Zn-acetate and Cu-acetate precursors solution.

Element	At. No.	Line s.	Netto	Mass [%]	Mass Norm. [%]	Atom [%]	Comp.	Sto. [%]	Sto. Norm.	Abs. error [%](3sigma)
Cu	29	K-series	25383	103.91	90.28	84.93		103.91	90.28	10.16
Sn	50	L-series	5186	6.43	5.58	2.81		6.43	5.58	0.73
Si	14	K-series	1953	1.40	1.22	2.59	SiO_2	2.99	2.60	0.29
Al	13	K-series	1234	0.93	0.81	1.80	Al_2O_3	1.76	1.53	0.25
C	6	K-series	5824	0.00	0.00	0.00		0.00	0.00	0.00
O	8	K-series	9830	2.42	2.11	7.87		0.00	0.00	1.10
Sum				**115.09**	**100**	**100**		**115.09**	**100.00**	

The spectrum identifies the presence of key elements, including copper (Cu), Zinc (Zn), oxygen (O), and traces of silicon (Si), tin (Sn), and aluminum (Al), with their respective atomic percentages summarized in the accompanying table. The copper (Cu) contributes the majority of the detected atomic composition, with a normalized atomic percentage of 90.28%. This dominant presence aligns with the dense and compact CuO layer observed in the SEM images, confirming its role as the primary *p*-type semiconductor in the heterostructure. The FTIR analysis described earlier further supports this by identifying Cu–O stretching vibrations (~660 cm^{-1}), indicating the formation of the CuO phase. Oxygen (O) atoms account for 7.87% of the total composition. This is consistent with the formation of both CuO and ZnO phases, as highlighted by the broad FTIR O–H stretching (~3402 cm^{-1}) and the M–O vibrations in the 600–660 cm^{-1} range. The relatively low percentage of oxygen may also reflect the presence of oxygen vacancies, which are known to enhance conductivity in oxide films, improving their suitability for energy applications. Though Zinc (Zn) not explicitly labeled in the spectrum provided, the absence of a significant zinc peak suggests that Zn content may be below the detection threshold or unevenly distributed due to co-deposition. However, FTIR results confirmed the ZnO phase through its Zn–O stretching vibrations (~600 cm^{-1}), and SEM images showed a granular ZnO morphology atop the CuO base. This disparity may arise from differences in the deposition rates or the limited incorporation of ZnO during simultaneous deposition. Other elements (Sn, Si, Al) traces of tin (6.43%) and silicon (2.81%) originate from the FTO substrate and underlying glass, respectively. Compared to similar heterojunctions like ZnO/CuO films prepared via sequential deposition (Kara *et al.*, 2019), (Yin *et al.*, 2022), the simultaneous deposition of FTO/CuO/ZnO films provides unique advantages. The co-deposition process ensures direct bonding between CuO and ZnO, minimizing interfacial defects and improving charge carrier separation. Additionally, the compact CuO layer and granular ZnO surface identified in SEM and FTIR analyses, combined with the oxygen vacancies suggested by EDS, enhance charge transport and photocatalytic efficiency. This combination of features makes FTO/CuO/ZnO films highly promising for energy harvesting applications, such as photovoltaic devices, photoelectrochemical water splitting, and thermoelectric.

3.3.3 Structural properties of FTO/CuO/ZnO heterostructure thin films from a common Zn- and Cu-acetate buffer solution

Figure 11 illustrates the XRD spectrum of electrodeposited FTO/CuO/ZnO heterostructures films reveals distinct crystalline phases indicative of a robust structural composition essential for energy harvesting applications. The diffraction peaks can be assigned to characteristic planes of CuO (e.g., (111), (200), and (202)) and ZnO (e.g., (100), (002), and (101)), as corroborated by the JCPDS cards

(CuO: 45-0937, ZnO: 36-1451). Additional reflections correspond to SnO_2 from the FTO substrate, as confirmed by EDS analysis. These results confirm the successful co-deposition of CuO and ZnO phases with crystal size 31.18 and 13.51 nm, respectively, and minimal presence of secondary phases or structural defects. The observed peak broadening and potential shifts highlight lattice strain at the CuO/ZnO interface, which could enhance defect density critical for tailoring electrical conductivity and band alignment. When benchmarked against similar systems such as CuO/ZnO films prepared via sequential deposition (Çetinel *et al.*, 2023), (Rosas-Laverde *et al.*, 2020), the co-deposited FTO/CuO/ZnO films exhibit distinct advantages in structural integrity and interfacial bonding.

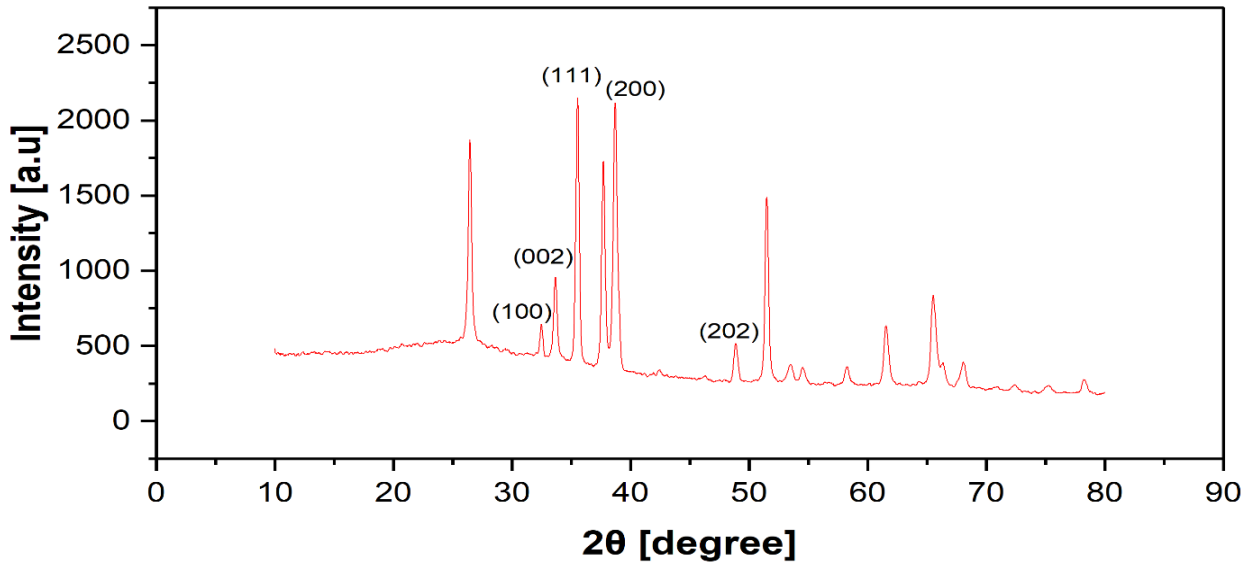

Figure 11. XRD spectrum of electrodeposited FTO/CuO/ZnO heterostructures films from a common Zn-acetate and Cu-acetate buffer solution.

The direct chemical interaction between CuO and ZnO, achieved during simultaneous deposition, reduces interfacial voids and defects, thereby improving charge carrier transport and separation efficiency. The complementary EDS, FTIR, and SEM analyses further underscore the structural and compositional uniqueness of the synthesized films. Compared to reported CuO/ZnO systems, where the presence of defects at the interfaces often hinders device performance, the co-deposited CuO/ZnO films demonstrate unique characteristics that are particularly advantageous for energy harvesting applications.The compact CuO layer serves as an efficient *p*-type semiconductor, ensuring effective light absorption and charge generation, while the granular ZnO morphology provides high surface area and promotes efficient charge transport. The direct chemical bonding between CuO and ZnO minimizes charge recombination, enhancing the overall energy conversion efficiency. Thus, the simultaneous electrodeposition of FTO/CuO/ZnO heterostructures films presents a highly promising approach for fabricating energy harvesting devices.

3.4 FTO/CuO/ZnO vs. FTO/CuO/ZnO heterostructures films from distinct and buffer precursors solution

The comparative analysis of FTO/CuO/ZnO heterostructures films from sequential and in-situ deposition, reveal distinct advantages and limitations for energy-harvesting applications. From distinct solution heterostructures of FTO/CuO/ZnO, characterized by their sequentially deposited CuO and ZnO layers, exhibit well-defined interfaces with minimal contamination, ensuring efficient charge transport and enhanced optoelectronic properties. The dense, uniform CuO base and granular ZnO

morphology enable optimal light absorption and charge separation, making these structures particularly suitable for high-efficiency photovoltaic and photocatalytic applications. In contrast, FTO/CuO/ZnO heterostructures prepared via simultaneous deposition from a buffer solution offer superior material homogeneity, reduced fabrication complexity, and better interfacial bonding. The compact CuO and partially pyramid-like ZnO morphology of heterostructure promote enhanced structural stability, light scattering, and surface area, crucial for thermoelectric and photoelectrochemical devices.

The structural and compositional integrity, as evidenced by XRD, EDS, FTIR, and SEM analyses, ensures superior optoelectronic properties, making these heterostructures a compelling candidate for advanced photovoltaic and photocatalytic applications. The FTIR and EDS analyses suggest that buffer solution films may retain residual organic species and exhibit lower oxygen content, indicating the potential for post-deposition treatments to further improve their properties. The distinct solution films, on the other hand, benefit from greater control over individual layer quality but may require more time and resources for fabrication. XRD results show that both structures achieve good crystallinity, with buffer films displaying notable interfacial strain that could enhance conductivity and band alignment. The hydrated surface and residual organic groups observed in FTIR spectra point to the importance of post-deposition treatments like annealing to optimize film crystallinity and reduce impurities. Compared to sequential deposition methods, simultaneous deposition offers superior interlayer connectivity, material homogeneity, and time efficiency. These features collectively enhance light absorption, carrier transport, and minimize recombination losses, as corroborated by the compact CuO and high-surface-area ZnO morphologies.

Both sequential and in-situ deposition of FTO/CuO/ZnO films demonstrate significant promise for energy harvesting, with each method offering unique advantages. Distinct solution heterostructures excel in precision and layer definition, making them ideal for applications requiring fine-tuned optoelectronic properties. Conversely, buffer solution films provide a cost-effective and scalable solution, with robust interfacial bonding and high structural integrity that are advantageous for large-scale implementations. Future research required focusing on optimizing the deposition conditions, addressing residual impurities, and tailoring the interface properties to maximize the performance of both configurations with their device applications. Combined with their scalability and adaptability, these heterostructures demonstrate a transformative step toward developing next-generation energy devices that balance efficiency, affordability, and environmental sustainability. The method's ability to produce defect-minimized interfaces with strong interfacial bonding makes it a promising pathway for next-generation optoelectronic and sustainable energy technologies. Thus, this work not only highlights the potential of co-deposition techniques for improving device performance but also sets the stage for further optimization in scalable and eco-friendly energy device fabrication processes.

Conclusion

A sustainable and efficient acetate-derived electrodeposition method for the scalable synthesis of ZnO and CuO and their heterostructures has been studied and analyzed systematically. The structural and compositional integrity, as evidenced by XRD, EDS, FTIR, and SEM analyses, ensures superior optoelectronic properties, making these heterojunctions a compelling candidate for both energy harvesting and photocatalytic applications. By optimizing deposition parameters, including potential, pH, and temperature, high-quality heterojunctions with enhanced photocatalytic and optoelectronic properties were achieved. Comparative analyses reveal that distinct solution FTO/CuO/ZnO films offer superior interfacial control toward application in optoelectronic devices, while deposition from ethylene glycol-based electrolytic solution containing both Zn and Cu-acetate salts solution

FTO/CuO/ZnO films provide scalable, cost-effective solutions for energy harvesting applications. Both structures exhibit competitive and promising performance, including enhanced light absorption, charge separation, and stability. This one-pot acetate-assisted heterostructure development approach simplifies fabrication strategy, minimizes contamination risks, while maintaining high performance, paving the way for environmentally friendly, scalable energy and environmental solutions in next-generation devices.

Acknowledgement: The authors acknowledge the international collaborative research program University of Rajshahi, Bangladesh, and Ritsumeikan University, Japan.
Disclosure statement: *Conflict of Interest:* The authors declare that there are no conflicts of interest.
Compliance with Ethical Standards: This article does not contain any studies involving human or animal subjects.

References

Al-Katrib, M., Perrin, L., Flandin, L. and Planes, E. 2023. Electrodeposition in perovskite solar cells: a critical review, new insights, and promising paths to future industrial applications. *Advanced Materials Technologies*. 8, 23 (Oct. 2023). https://doi.org/10.1002/admt.202300964.

Alshahateet S.F., Al-Trawneh S.A., Er-rajy M., Zerrouk M., Azzaoui K., *et al*. 2024. Green Synthesis of Zinc Oxide Nanoparticles for Tetracycline Adsorption: Experimental Insights and DFT Study. *Plants*, 13(23), 3386. https://doi.org/10.3390/plants13233386

Amiri, M. and Bélanger, D. 2021. Zinc electrodeposition in acetate-based Water-in-Salt electrolyte: Experimental and theoretical studies. *ChemElectroChem*. 8, 14 (Jun. 2021), 2737–2745. https://doi.org/10.1002/celc.202100541.

Asim, N., Ahmadi, S., Alghoul, M.A., Hammadi, F.Y., Saeedfar, K. and Sopian, K. 2014. Research and development aspects on chemical preparation techniques of photoanodes for dye sensitized solar cells. *International Journal of Photoenergy*. 2014, (Jan. 2014), 1–21. https://doi.org/10.1155/2014/518156.

Aswada, A.T., Abbasa, A.T., Alib, G.G. Effect of deposition time on optical properties of CuO thin film prepared by chemical bath deposition method. *Digest Journal of Nanomaterials and Biostructures* Vol. 16, No. 3, July - September 2021, p. 831 – 838

Badalbayli, A., Sinclair, N., Bernasconi, R., Borisenko, N., Venkatesh, K., Ispas, A., Akolkar, R. and Magagnin, L. 2024. Advancements in electrodeposition for precise manufacturing and sustainability. *The Electrochemical Society Interface*. 33, 2 (Jun. 2024), 47–54. https://doi.org/10.1149/2.f09242if.

Bahnasawy, N., Elbanna, A.M., Ramadan, M. and Allam, N.K. 2022. Fabrication of polyhedral Cu–Zn oxide nanoparticles by dealloying and anodic oxidation of German silver alloy for photoelectrochemical water splitting. *Scientific Reports*. 12, 1 (Oct. 2022). https://doi.org/10.1038/s41598-022-21127-1.

Bekru, A.G., Tufa, L.T., Zelekew, O.A., Goddati, M., Lee, J. and Sabir, F.K. 2022. Green synthesis of a CUO–ZNO nanocomposite for efficient photodegradation of methylene blue and reduction of 4-Nitrophenol. *ACS Omega*. 7, 35 (Aug. 2022), 30908–30919. https://doi.org/10.1021/acsomega.2c02687.

Bouachma, S., Ayouz-Chebout, K., Kechouane, M., Manseri, A., Yaddadene, C., Menari, H. and Gabouze, N. 2021. Synthesis of PSi-n/CuO-p/Cu2O-n heterostructure for CO2 gas sensing at room temperature. *Applied Physics A*. 128, 1 (Dec. 2021). https://doi.org/10.1007/s00339-021-05167-4.

Casabán, J., Hardacre, C., James, S.L. and Lagunas, M.C. 2012. A more direct way to make catalysts: one-pot ligand-assisted aerobic stripping and electrodeposition of copper on graphite. *Green Chemistry*. 14, 6 (Jan. 2012), 1643. https://doi.org/10.1039/c2gc35147a.

Çetinel, A. and Utlu, G. 2023. Preparation and characterization of electrochemically deposited CU2O/ZNO heterojunctions on porous silicon. *ACS Omega*. 8, 23 (May 2023), 20801–20809. https://doi.org/10.1021/acsomega.3c01438.

Chatterjee, S. and Pal, A.J. 2016. Introducing CU2O thin films as a Hole-Transport layer in efficient planar perovskite solar cell structures. *The Journal of Physical Chemistry C*. 120, 3 (Jan. 2016), 1428–1437. https://doi.org/10.1021/acs.jpcc.5b11540.

Costas, A., Florica, C., Preda, N., Besleaga, C., Kuncser, A. and Enculescu, I. 2022. Self-connected CuO–ZnO radial core–shell heterojunction nanowire arrays grown on interdigitated electrodes for visible-light photodetectors. *Scientific Reports*. 12, 1 (Apr. 2022). https://doi.org/10.1038/s41598-022-10879-5.

Costas, A., Florica, C., Preda, N., Kuncser, A. and Enculescu, I. 2020. Photodetecting properties of single CuO–ZnO core–shell nanowires with p–n radial heterojunction. *Scientific Reports*. 10, 1 (Oct. 2020). https://doi.org/10.1038/s41598-020-74963-4.

Cui, J. and Gibson, U.J. 2010. A simple Two-Step electrodeposition of CU2O/ZNO nanopillar solar cells. *The Journal of Physical Chemistry C*. 114, 14 (Mar. 2010), 6408–6412. https://doi.org/10.1021/jp1004314.

Dehaj, M.S. and Mohiabadi, M.Z. 2019. Experimental study of water-based CuO nanofluid flow in heat pipe solar collector. *Journal of Thermal Analysis and Calorimetry*. 137, 6 (Mar. 2019), 2061–2072. https://doi.org/10.1007/s10973-019-08046-6.

Deora, S.M. and Sharma, K.S. Structural, morphological and optical studies of nanocrystalline CuO thin films by solution processed Spin Coating technique. © *2019 JETIR* January 2019, Volume 6, Issue 1 www.jetir.org (ISSN-2349-5162)

Escorcia-Díaz, D., García-Mora, S., Rendón-Castrillón, L., Ramírez-Carmona, M. and Ocampo-López, C. 2023. Advancements in Nanoparticle deposition Techniques for diverse Substrates: A review. *Nanomaterials*. 13, 18 (Sep. 2023), 2586. https://doi.org/10.3390/nano13182586.

Filopoulou, A., Vlachou, S. and Boyatzis, S.C. 2021. Fatty acids and their metal salts: A review of their infrared spectra in light of their presence in cultural heritage. *Molecules*. 26, 19 (Oct. 2021), 6005. https://doi.org/10.3390/molecules26196005.

Ghimire, R.R., Pokhrel, B.P., Gupta, S.P., Joshi, L.P. and Rai, K.B. 2023. Optical and electrical properties of homo and heterojunction formed by the ZNO/FTO and CUO/ZNO/FTO nanostructures. *Journal of Nepal Physical Society*. 9, 1 (Aug. 2023), 73–82. https://doi.org/10.3126/jnphyssoc.v9i1.57600.

Hajji, M., Dabbabi, S., Ajili, M., Jebbari, N., Loureiro, A.G. and Kamoun, N.T. 2024. Investigations on physical properties of CuO–ZnO couple oxide sprayed thin films for environmental applications (ozone gas sensing and MB degradation). *Journal of Materials Science Materials in Electronics*. 35, 9 (Mar. 2024). https://doi.org/10.1007/s10854-024-12427-5.

Hssi, A.A., Atourki, L., Labchir, N., Ouafi, M., Abouabassi, K., Elfanaoui, A., Ihlal, A. and Bouabid, K. 2020. Optical and dielectric properties of electrochemically deposited p-Cu2O films. *Materials Research Express*. 7, 1 (Jan. 2020), 016424. https://doi.org/10.1088/2053-1591/ab6772.

Hussain, S., Cao, C., Nabi, G., Khan, W.S., Usman, Z. and Mahmood, T. 2011. Effect of electrodeposition and annealing of ZnO on optical and photovoltaic properties of the p-Cu2O/n-ZnO solar cells. *Electrochimica Acta*. 56, 24 (Jul. 2011), 8342–8346. https://doi.org/10.1016/j.electacta.2011.07.017.

Imani, M., Safaei, M., Moradpoor, H., Rezaei, R., Golshah, A., Rezaei, F. and Jamshidy, L. 2020. Optimum synthesis of CuO nanoparticles with the highest antifungal activity against oral pathogen Candida albicans. *Journal of Applied Pharmaceutical Science*. 10, 2 (Feb. 2020), 21–25. https://doi.org/10.7324/japs.2020.102004.

Izaki, M., Hisamatsu, R., Saito, T., Murata, K., Sasano, J. and Shinagawa, T. 2014. Hybrid zinc oxide:Cu-phthalocyanine bulk-heterojunction photovoltaic device. *RSC Advances*. 4, 29 (Jan. 2014), 14956–14961. https://doi.org/10.1039/c4ra01051e.

Jayswal, S. and Moirangthem, R.S. 2018. Thermal decomposition route to synthesize ZnO nanoparticles for photocatalytic application. *AIP Conference Proceedings*. (Jan. 2018). https://doi.org/10.1063/1.5052092.

Jeong, S.S., Mittiga, A., Salza, E., Masci, A. and Passerini, S. 2007. Electrodeposited ZnO/Cu2O heterojunction solar cells. *Electrochimica Acta*. 53, 5 (Sep. 2007), 2226–2231. https://doi.org/10.1016/j.electacta.2007.09.030.

Jrajri, K., Beraich, M., Warad, I., Guenbour, A., Bellaouchou, A. and Zarrouk, A. 2021. Electrodeposition of Cu2O thin Film Onto Copper Substrate by Linear Sweep Voltammetry at Low Duration: Effect of Bath pH. *Biointerface Research in Applied Chemistry*. 12, 6 (Nov. 2021), 7715–7724. https://doi.org/10.33263/briac126.77157724.

Kaphle, A., Echeverria, E., Mcllroy, D.N. and Hari, P. 2020. Enhancement in the performance of nanostructured CuO–ZnO solar cells by band alignment. *RSC Advances*. 10, 13 (Jan. 2020), 7839–7854. https://doi.org/10.1039/c9ra10771a.

Kara, R., Boudoukha,D., Azizi, A. Effect of i-ZnO seed layer on the properties of electrodeposited p-Cu2O/nZnO/FTO heterojunction thin films. *Transactions on Nanotechnology*.

Khan, Z.R., Khan, M.S., Zulfequar, M. and Khan, M.S. 2011. Optical and structural properties of ZNO thin films fabricated by Sol-Gel Method. *Materials Sciences and Applications*. 02, 05 (Jan. 2011), 340–345. https://doi.org/10.4236/msa.2011.25044.

Khan, M., Ansari, A., Hameedullah, M. *et al.* Sol-gel synthesis of thorn-like ZnO nanoparticles endorsing mechanical stirring effect and their antimicrobial activities: Potential role as nano-antibiotics. *Sci Rep* **6**, 27689 (2016). https://doi.org/10.1038/srep27689

Kidowaki, H., Oku, T. and Akiyama, T. 2012. Fabrication and characterization of CuO/ZnO solar cells. *Journal of Physics Conference Series*. 352, (Mar. 2012), 012022. https://doi.org/10.1088/1742-6596/352/1/012022.

Kumar, M. and Sasikumar, C. 2014. Electrodeposition of Nanostructured ZNO Thin Film: A review. *American Journal of Materials Science and Engineering*. 2, 2 (May 2014), 18–23. https://doi.org/10.12691/ajmse-2-2-2.

Lahmar, H., Setifi, F., Azizi, A., Schmerber, G. and Dinia, A. 2017. On the electrochemical synthesis and characterization of p-Cu2O/n-ZnO heterojunction. *Journal of Alloys and Compounds*. 718, (May 2017), 36–45. https://doi.org/10.1016/j.jallcom.2017.05.054.

Li B., Wang Y. (2010). Facile synthesis and photocatalytic activity of ZnO–CuO nanocomposite. *Superlattices and Microstructures*. 47, 5 (Mar. 2010), 615–623. https://doi.org/10.1016/j.spmi.2010.02.005.

Mezine, Z., Kadri, A., Hamadou, L., Benbrahim, N. and Chaouchi, A. 2018. Electrodeposition of copper oxides (CuxOy) from acetate bath. *Journal of Electroanalytical Chemistry*. 817, (Mar. 2018), 36–47. https://doi.org/10.1016/j.jelechem.2018.03.055.

Mia, N.H., Rana, S.M., Pervez, F., Rahman, M.R., Hossain, K., Mortuza, A.A., Basher, M.K. and Hoq, M. 2017. Preparation and spectroscopic analysis of zinc oxide nanorod thin films of different thicknesses. *Materials Science-Poland*. 35, 3 (Oct. 2017), 501–510. https://doi.org/10.1515/msp-2017-0066.

Murzin, S.P. 2022. Formation of ZNO/CUO heterostructures based on Quasi-One-Dimensional nanomaterials. *Applied Sciences*. 13, 1 (Dec. 2022), 488. https://doi.org/10.3390/app13010488.

Muthukumar, A., Rey, G., Giusti, G., Consonni, V., Appert, E., Roussel, H., Dakshnamoorthy, A., Bellet, D. 2013. Fluorine doped tin oxide (FTO) thin film as transparent conductive oxide (TCO) for photovoltaic applications. *AIP Conference Proceedings*. (Jan. 2013). https://doi.org/10.1063/1.4791235.

Oliveira, F.F., Proenca, M.P., Araújo, J.P. and Ventura, J. 2016. Electrodeposition of ZnO thin films on conducting flexible substrates. *Journal of Materials Science*. 51, 12 (Mar. 2016), 5589–5597. https://doi.org/10.1007/s10853-016-9850-6.

Ozer, Z.N., Ozkan, M. and Pat, S. 2024. Optical and electric characteristics of CuO nanoparticle-doped ZnO thin films using thermionic vacuum arc deposition system. *Journal of Materials Science Materials in Electronics*. 35, 6 (Feb. 2024). https://doi.org/10.1007/s10854-024-12158-7.

Pedersen, H., Barry, S.T. and Sundqvist, J. 2021. Green CVD—Toward a sustainable philosophy for thin film deposition by chemical vapor deposition. *Journal of Vacuum Science & Technology a Vacuum Surfaces and Films*. 39, 5 (Jul. 2021). https://doi.org/10.1116/6.0001125.

Pena, E.M.D. and Roy, S. 2018. Electrodeposited copper using direct and pulse currents from electrolytes containing low concentration of additives. *Surface and Coatings Technology*. 339, (Feb. 2018), 101–110. https://doi.org/10.1016/j.surfcoat.2018.01.067.

Rana, P., Biswas, K.P., Tabassum, S., Rahman, F., Ismail, M.B.A. Exploring Deposition Temperature-Tailored Structural and Morphological Transformations in Electrochemically Deposited PbOx on Cu Substrate with Acetate-Electrolyte, *J. Mater. Environ. Sci.*, 2024, Volume 15, Issue 8, Page 1127-1137

Rosas-Laverde, N., Pruna, A., Cembrero, J. and Busquets-Mataix, D. 2020. Electrodeposition of ZNO/CU2O heterojunctions on NI-MO-P electroless coating. *Coatings*. 10, 10 (Sep. 2020), 935. https://doi.org/10.3390/coatings10100935.

Saji, K.J., Populoh, S., Tiwari, A.N. and Romanyuk, Y.E. 2013. Design of p-CuO/n-ZnO heterojunctions by rf magnetron sputtering. *Physica Status Solidi (A)*. 210, 7 (Mar. 2013), 1386–1391. https://doi.org/10.1002/pssa.201228293.

Saji, K.J., Populoh, S., Tiwari, A.N. and Romanyuk, Y.E. 2013. Design of p-CuO/n-ZnO heterojunctions by rf magnetron sputtering. *Physica Status Solidi (A)*. 210, 7 (Mar. 2013), 1386–1391. https://doi.org/10.1002/pssa.201228293.

Septina, W., Ikeda, S., Khan, M.A., Hirai, T., Harada, T., Matsumura, M. and Peter, L.M. 2011. Potentiostatic electrodeposition of cuprous oxide thin films for photovoltaic applications. *Electrochimica Acta*. 56, 13 (Feb. 2011), 4882–4888. https://doi.org/10.1016/j.electacta.2011.02.075.

Shaikh, A.V., Sayyed, S.G., Naeem, S. and Mane, R.S. 2020. Electrodeposition of N-CDSE/P-CU2SE heterojunction solar cells. *Engineered Science*. (Jan. 2020). https://doi.org/10.30919/es8d1124.

Shin, S., Park, C., Kim, C., Kim, Y., Park, S. and Lee, J.-H. 2015. Cyclic voltammetry studies of copper, tin and zinc electrodeposition in a citrate complex system for CZTS solar cell application. *Current Applied Physics*. 16, 2 (Dec. 2015), 207–210. https://doi.org/10.1016/j.cap.2015.11.017.

Siddiqui, H., Parra, M.R., Qureshi, M.S., Malik, M.M., Haque, F.Z. 2018. Studies of structural, optical, and electrical properties associated with defects in sodium-doped copper oxide (CuO/Na) nanostructures. *Journal of Materials Science*. 53, 12, 8826–8843. https://doi.org/10.1007/s10853-018-2179-6.

Siregar, N., Motlan, M. and Sirait, M. 2023. Electroplated ZNO Thin Film: Influence of deposition time on optical and structural properties. *Journal of Physical Science*. 34, 1 (Apr. 2023), 43–55. https://doi.org/10.21315/jps2023.34.1.4.

Siva, V., Murugan, A., Shameem, A.S. and Bahadur, S.A. 2020. One-step hydrothermal synthesis of transition metal oxide electrode material for energy storage applications. *Journal of Materials Science Materials in Electronics*. 31, 22 (Oct. 2020), 20472–20484. https://doi.org/10.1007/s10854-020-04566-2.

Slimani, H., Bessous, N., Dagher, S., Hilal-Alnaqbi, A., Gamal, M.E., Akhozheya, B. and Mohammed, M. 2020. Growth of ZnO nanorods on FTO glass substrate. *Materials Research Express*. 7, 2 (Feb. 2020), 025026. https://doi.org/10.1088/2053-1591/ab727b.

Stalcup, M., Gayoso, V. and Watkins, T.S. 2024. Optimization of Acetate-Based electrochemical baths for electrochemical deposition of high purity molybdenum. *Meeting Abstracts/Meeting Abstracts (Electrochemical Society. CD-ROM)*. MA2024-01, 25 (Aug. 2024), 1442. https://doi.org/10.1149/ma2024-01251442mtgabs.

Šulčiūtė, A. and Valatka, E. 2012. Electrodeposition and photoelectrocatalytic activity of ZNO films on AISI 304 type steel. *Materials Science*. 18, 4 (Dec. 2012). https://doi.org/10.5755/j01.ms.18.4.3089.

Suleiman M., Mousa M., Hussein A., Hammouti B., Hadda T. B., Warad I. (2013) Copper(II)-Oxide Nanostructures: Synthesis, Characterizations and their Applications–Review, *J. Mater. Environ. Sci.* 4 (5), 792-797

Sydnes, M. 2014. One-Pot Reactions: A step towards greener chemistry. *Current Green Chemistry*. 1, 3 (Feb. 2014), 216–226. https://doi.org/10.2174/2213346101666140221225404.

Tolosa, M.D.R., Alajami, M., Reguera, A.E.M., Damonte, L.C. and Hernández-Fenollosa, M.A. 2019. Influence of seed layer thickness on properties of electrodeposited ZnO nanostructured films. *SN Applied Sciences*. 1, 10 (Sep. 2019). https://doi.org/10.1007/s42452-019-1293-7.

Tran, M.H., Cho, J.Y., Sinha, S., Gang, M.G. and Heo, J. 2018. Cu2O/ZnO heterojunction thin-film solar cells: the effect of electrodeposition condition and thickness of Cu2O. *Thin Solid Films*. 661, (Jul. 2018), 132–136. https://doi.org/10.1016/j.tsf.2018.07.023.

Varughese, A., Kaur, R. and Singh, P. 2020. Green Synthesis and Characterization of Copper Oxide Nanoparticles Using Psidium guajava Leaf Extract. *IOP Conference Series Materials Science and Engineering*. 961, 1 (Nov. 2020), 012011. https://doi.org/10.1088/1757-899x/961/1/012011.

Vasiliev, M., Nur-E-Alam, M. and Alameh, K. 2019. Recent developments in solar Energy-Harvesting technologies for building integration and distributed energy generation. *Energies*. 12, 6 (Mar. 2019), 1080. https://doi.org/10.3390/en12061080.

Walsh, F.C. 1991. The overall rates of electrode reactions: Faraday's Laws of Electrolysis. *Transactions of the IMF*. 69, 4 (Jan. 1991), 155–157. https://doi.org/10.1080/00202967.1991.11870914.

Yin, T.-H., Liu, B.-J., Lin, Y.-W., Li, Y.-S., Lai, C.-W., Lan, Y.-P., Choi, C., Chang, H.-C. and Choi, Y. 2022. Electrodeposition of Copper Oxides as Cost-Effective heterojunction photoelectrode materials for solar water splitting. *Coatings*. 12, 12 (Nov. 2022), 1839. https://doi.org/10.3390/coatings12121839.

Zhang, L., Cui, J., Zhang, Y., San, X. and Meng, D. 2023. Surface conversion of CuO–ZnO to ZIF-8 to enhance CO2adsorption for CO2hydrogenation to methanol. *New Journal of Chemistry*. 47, 14 (Jan. 2023), 6700–6707. https://doi.org/10.1039/d2nj05832d.